ARTICLE

Understanding Photolysis of CH_3ONO_2 with On-the-Fly Nonadiabatic Dynamics Simulation at the ADC(2) Level[†]

Juanjuan Zhang[a,b], Jiawei Peng[a,d], Deping Hu[c*], Chao Xu[a,b*], Zhenggang Lan[a,b*]

a. SCNU Environmental Research Institute, Guangdong Provincial Key Laboratory of Chemical Pollution and Environmental Safety & MOE Key Laboratory of Environmental Theoretical Chemistry, South China Normal University, Guangzhou 510006, China
b. School of Environment, South China Normal University, Guangzhou 510006, China
c. Department of Chemistry, University of Rochester, Rochester, New York 14627, USA
d. School of Chemistry, South China Normal University, Guangzhou 510006, China

(Dated: Received on January 17, 2022; Accepted on March 17, 2022)

The nonadiabatic dynamics of methyl nitrate (CH_3ONO_2) is studied with the on-the-fly trajectory surface hopping dynamics at the ADC(2) level. The results confirmed the existence of the ultrafast nonadiabatic decay to the electronic ground state. When the dynamics starts from S_1 and S_2, the photoproducts are CH_3O+NO_2, consistent with previous results obtained from the experimental studies and theoretical dynamics simulations at more accurate XMS-CASPT2 level. The photolysis products are CH_3O+NO_2 at the ADC(2) level when the dynamics starts from S_3, while different photolysis products were obtained in previous experimental and theoretical works. These results demonstrate that the ADC(2) method may still be useful for treating the photolysis mechanism of CH_3ONO_2 at the long-wavelength UV excitation, while great caution should be paid due to its inaccurate performance in the description of the photolysis dynamics at the short-wavelength UV excitation. This gives valuable information to access the accuracy when other alkyl nitrates are treated at the ADC(2) level.

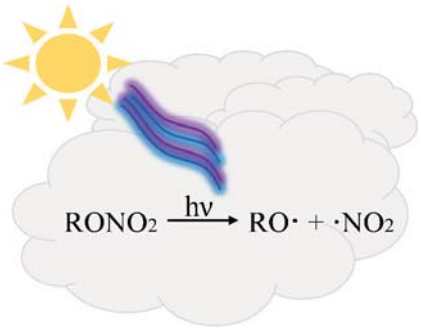

Key words: Alkyl nitrate, Nonadiabatic dynamics, Photolysis, Conical intersection, Volatile organic compound

I. INTRODUCTION

Volatile organic compounds (VOCs) are well-known atmospheric pollutants that cause negative impacts on living beings and environment [1–9]. As a typical and simple VOC containing nitrogen, methyl nitrate (CH_3ONO_2) displays the good thermal stability in the atmosphere [10–13], and its UV photolysis produces NO_x [13, 14] (a group of well-known pollutant compounds). Therefore, the thermal reactions and photochemistry of CH_3ONO_2 and other alkyl nitrates attract considerable attentions in experimental and theoretical studies [12–27].

The UV absorption spectra of CH_3ONO_2 [11, 12, 16, 18, 23, 26, 28] show a strong band around 190−220 nm, along with a weaker band that extends to 330 nm. The diffused absorption bands indicate that the lifetime of the excited states should be extremely short. This well-known relationship between the peak width in the absorption spectra and the excited-state lifetime in the

[†]Part of Special Topic "Quantum and Classical Dynamics in Chemistry Symposium in the 32nd Chinese Chemical Society Congress".

*Authors to whom correspondence should be addressed. E-mail: dhu13@ur.rochester.edu, chaoxu@m.scnu.edu.cn, zhenggang.lan@m.scnu.edu.cn

DOI:10.1063/1674-0068/cjcp2201013

nonadiabatic dynamics were clearly discussed in the book "Conical Intersections" [29, 30]. Different photoproducts are formed upon the UV excitation at different wavelengths, as confirmed in previous works [11, 14, 18, 22]. For example, Yang *et al.* [14] found the photolysis products are mainly CH_3O+NO_2 at 248 nm, two main channels (CH_3O+NO_2 and CH_3O+NO+O) and a minor channel (CH_3ONO+O) appear at 193 nm. Talukdar *et al.* [18] found that the photoproducts are mainly CH_3O+NO_2 at 248 nm and 308 nm, and the O atom is observed at 193 nm. Similar photolysis features were also found in other experimental works [11, 31]. In the theoretical study, Soto, Arenas, and coworkers [22] explored different channels, such as CH_3O+NO_2 and CH_3ONO+O, by building excited-state potential energy surfaces (PESs) at the multi-state complete active space second order perturbation theory (MS-CASPT2) level. They also discussed the quasi-degeneracy of the low-lying electronic states in the dissociation limit from the symmetry perspective. Apart from these works, there are many valuable experimental and theoretical studies on other alkyl nitrates and their derivatives, which show the similar photolysis reactions [10, 11, 16, 18, 23, 26, 31–36].

In the previous work [37], we provided the first all-atomic-level simulation of the excited-state nonadiabatic dynamics of CH_3ONO_2 using the on-the-fly trajectory surface hopping (TSH) method [38] at the high-level electronic-structure theory, namely, the extended multi-state complete active space second order perturbation theory with the def2-SVPD basis set (XMS(4)-CASPT2(12,9)/def2-SVPD) [39–41]. The two lowest excited states S_1 and S_2 are dark states, which correspond to n$\rightarrow\pi^*$ and n/$\sigma\rightarrow\pi^*$ transition, respectively. The third excited state S_3 is the bright state and responsible for the strong UV absorption, which is dominated by the $\pi\rightarrow\pi^*$ transition. When any of these three states is excited, the ultrafast interval conversion to the ground state takes place via S_1/S_0 conical intersection, and then the large excessive energy leads to the further dissociation on the ground state. When the long UV excitation wavelength is considered or the dynamics starts from the low-lying excited states S_1 and S_2, the main photolysis channel is to produce CH_3O+NO_2, the state degeneracy exists in this dissociation limit. When the UV excitation at the short wavelength is considered and the S_3 is reachable, both CH_3O+NO_2 and CH_3O+NO+O channels become equally important; the third channel CH_3ONO+O is also observed, while the branching ratio is very low. The dependence of the photolysis channels on the UV excitation wavelength in our simulation qualitatively agrees with available experimental studies.

The CH_3ONO_2 compound is small, which only contains eight atoms. Therefore, it is possible to simulate excited-state nonadiabatic dynamics of CH_3ONO_2 at the high-accurate levels of theories. The advantage to employ the XMS-CASPT2 method in the treatment of the excited-state nonadiabatic dynamics is rather clear. Normally, the XMS-CASPT2 method provides enough accuracy in the calculations of the excited states of polyatomic systems [4, 42, 43]. As a multi-configuration theory, it gives reasonable description of the chemical process that involves bond cleavages, biradicals formation, and conical-intersections decay. However, its shortcoming is also obvious. For instance, the computational cost becomes extremely high with the increasing of the system size. In addition, the XMS-CASPT2 results strongly depend on the calculation setups, such as the active space and state average, while the proper selection of them is not a trivial task. Although the XMS-CASPT2 method may give the proper description of the nonadiabatic dynamics of very small alkyl nitrates (such as CH_3ONO_2), currently it is almost not possible to use it to deal with the important photoinduced reactions of other alkyl nitrates and derivatives due to the large system size. Since the photochemical processes of alkyl nitrates and derivatives are very significant in environmental science, it is necessary to find a proper electronic-structure approach with suitable accucary and affordable computational cost in the theoretical description of their nonadiabatic dynamics.

Since the photolysis dynamics of alkyl nitrates involves the S_1/S_0 conical intersections, it is certainly preferable to employ the multi-reference theories to characterize the nonadiabatic decay. Therefore, other multi-reference theories, such as the multireference configuration interaction (MRCI) [44, 45] and the state-averaged complete active space self-consistent field (SA-CASSCF) [46, 47], may also be the possible choices, while they also suffer from the high computational cost [48, 49]. The semi-empirical OM2/MRCI method [50] may also be applicable, while its performance is also highly dependent on the system under study [51–54].

In recent years, we also noticed that the single reference theories, such as the time dependent density func-

DOI:10.1063/1674-0068/cjcp2201013

tional theory (TD-DFT) [55, 56] and the algebraic diagrammatic construction method to the second order (ADC(2)) [57, 58], were often used in the simulation of the nonadiabatic dynamics involving the S_1/S_0 conical intersections [59–64]. The advantages to select these methods are rather transparent, for instance, they require much less computational cost than multi-reference theories, and they are generally performed in a rather black-box way. In addition, they normally provide the reasonable treatment of the nonadiabatic decay dynamics, such as lifetime and dominant molecular motions, although they cannot provide an accurate description of the double-cone topologies of the S_1/S_0 conical intersections [61, 62, 65]. If these approaches can be used in the qualitative treatment of the nonadiabatic dynamics of alkyl nitrates, we may obtain the systematic understanding of their photochemistry.

The response theory ADC(2) gives a reasonable description of the excited states of polyatomic molecular systems, as discussed in previous works [63, 66, 67]. Although, the widely-used TD-DFT approaches may also be possible choices, it is well known that the TD-DFT results are highly dependent on the functional selection, and it may suffer from the improper treatment of the charge-transfer (CT) states with some functionals [68, 69]. In contrast, the ADC(2) method performs well in the treatment of the CT states. As the ADC(2) method gives the description of the excited-state pathway with the balance of computational cost and accuracy, several works used it to conduct the nonadiabatic dynamics simulations [4, 63, 70]. However, it seems that its performance is system-dependent. For instance, Barbatti, Lischka, and coworkers [67] once studied the nonadiabatic dynamics of the 9H-adenine at different levels of theories and concluded that the ADC(2) simulation correctly predicts the ultrafast deactivation process. Du and Lan [71] investigated the nonadiabatic dynamics of 10-hydroxybenzo[h]quinoline at the ADC(2) level, which confirmed that ADC(2) performs well in such large-sized molecules. Curchod and coworkers [72] studied nonadiabatic dynamics of thiophene and bithiophene at ADC(2) and TD-DFT levels. The results indicated that ADC(2) performs better than TD-DFT, and the ADC(2) method may be an attractive alternative approach to replace expensive multi-configuration theories in medium systems. Milovanović and coworkers [73] explored the photoinduced dynamics of uracil and uracil-water clusters at the ADC(2) level. The simulated excited-state dynamics is consistent with experimental observations. However, in other types of compounds, the ADC(2) results are not very convincing. For example, Hu *et al.* [62] investigated the nonadiabatic dynamics of keto isocytosine at both SA-CASSCF and ADC(2) levels, while these two methods give different excited-state dynamics. By benchmark calculations at high-level excited-state methods (MR-CISD and MS-CASPT2), it is found that SA-CASSCF results are more reasonable. Curchod and coworkers [74] reported that the systematic errors may exist in the description of the S_1/S_0 crossing of carbonyl containing compounds in the ADC(2) treatments. Overall, it seems that the accuracies of the ADC(2) treatments on the nonadiabatic dynamics are dependent on systems under study.

If the ADC(2) method can provide the reasonable treatment of the photolysis dynamics of alkyl nitrates and derivatives, the photochemistry of these compound families can be clarified without the involvement of multi-reference methods. This may open more opportunities to examine important environmental photochemistry of VOCs. However, it is necessary to perform benchmark calculations to examine the applicability of the ADC(2) approach in the treatment of these systems. Therefore, we study the nonadiabatic dynamics of CH_3ONO_2 with the TSH approach at the ADC(2) level. By comparing the current results with our previous ones obtained using the more accurate XMS-CASPT2 approach, we may access the accuracy of the ADC(2) in the theoretical treatment of the excited-state photolysis of CH_3ONO_2.

In a word, as a high-accurate level of theory, the XMS-CASPT2 method is certainly able to give the proper description of the excited-state nonadiabatic dynamics, while only for very small molecular systems. With the increasing of the system size, the computational cost quickly becomes extremely high and the results are also highly dependent on the computational setups. Thus, it is true that we can use the XMS-CASPT2 method to study the simplest alkyl nitrates (CH_3ONO_2), while the same calculations become very hard for larger systems. However, it is necessary to study other alkyl nitrates and more complicated derivatives because of their important roles in environmental science. Thus, we must find some applicable electronic-structure methods with the balance of the computational efficiency and the accuracy in order to study the photoinduced dynamics of methyl nitrate and deriva-

DOI:10.1063/1674-0068/cjcp2201013

tives. This is the main purpose of the current work. Our long-term goal is to study the excited-state dynamics of the methyl nitrate and derivatives, while these systems share many geometrical similarities and such features are well captured by the methyl nitrate (CH_3ONO_2). Therefore, we believe that it is enough to take such system to conduct the current benchmark calculations.

II. COMPUTATION DETAILS

The ground-state minimum-energy geometry (S_0-min shown in FIG. 1) of CH_3ONO_2 was optimized at the B3LYP/6-311+G(d) level with Gaussian 16 package [75]. The single-point excited state calculations at S_0-min were performed at the ADC(2) level of theory.

The lowest excited-state minimum-energy geometry (S_1-min) optimization and PESs were calculated at the ADC(2) level. We employed the linear interpolations in internal coordinates (LIIC) to construct the PESs from S_0-min to S_1-min. Starting from S_1-min, the PES scan along the stretching of the CH_3O-NO_2 bond was also conducted.

The on-the-fly TSH method with Tully's fewest-switches algorithm [38] was taken to simulate the ultrafast nonadiabatic dynamics of CH_3ONO_2 at the ADC(2) level. With the Wigner sampling [76] of the lowest vibrational state of the ground state minimum, the initial geometries and velocities were generated. Next, all snapshots were vertically placed to the excited state to start the nonadiabatic dynamics simulation.

The velocity-Verlet algorithm was employed to propagate the nuclear motion up to 250 fs with a time step of 0.5 fs, and the electronic motion was integrated with the unitary propagator with a time step of 0.005 fs. We set the parameter as 0.1 Hartree [77] in the decoherence correction approach proposed by Granucci and Persico [78]. The numerical nonadiabatic coupling terms were constructed numerically and all details were given in our previous works [62, 71]. Finally, 100 trajectories were performed for the dynamics initialized from S_1, S_2, and S_3, respectively. The ADC(2) method is essentially a single-reference theory. When the ground-state wavefunction is dominated by the open-shell configuration, the excitation energies become negative because the close-shell configuration no longer gives the lowest energy. In this case, we need to adjust the order of all electronic states according to their energies, *i.e.*, S_0, S_1, S_2, and S_3 always refer to the adiabatic states following the energy order. All dynamics calculations, as well as the numerical calculations of nonadiabatic couplings at the ADC(2) level, were performed with the JADE package [71, 79], which includes the interface between the TSH dynamics and the ADC(2) calculations in TURBOMOLE [80]. For all ADC(2) calculations, we selected the def2-TZVP basis set.

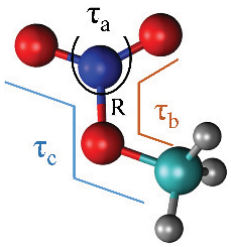

FIG. 1 The ground-state minimum-energy geometry of methyl nitrate (CH_3ONO_2). The O−N bond length and the O−O−O−N dihedral angle are shown as R and τ_a, respectively. The dihedral angles C−O−N−O (orange polyline τ_b) and C−O−N−O (blue polyline τ_c) describe the tortion at two O atoms, respectively.

III. RESULTS AND DISCUSSION

A. S_0-min and S_1-min

FIG. 2 (a) and (b) show the optimized geometries S_0-min and S_1-min, respectively. At S_0-min, the dihedral angle of O−O−O−N is 0°, and the geometry shows C_s symmetry. The N−O bonds of NO_2 are 1.21 Å and 1.20 Å, respectively. A similar S_0-min geometry was found in the previous work [81]. At S_0-min, the vertical excitation energies of S_1, S_2, and S_3 at the ADC(2)/def2-TZVP level are 4.74, 5.76, and 6.42 eV, respectively. In Table I, S_1 and S_2 are both dark, which are characterized by the n→π^* and σ/n→π^* transitions, respectively. S_3 is the lowest bright state, and it corresponds to the π→π^* transition. These properties of excited states at S_0-min are consistent with previous works [22, 26]. In fact, the oscillator strengths of S_1 and S_2 are very small, as shown in Table I. However, the oscillator strengths of them are not exactly zero. As the results, the experimental works still detect photolysis products at 220−300 nm in the UV absorption spectra [14, 18]. This clearly indicates that the dynamics starting from the lowest two excited states is important.

At S_1-min, the strong pyramidalization at the N atom is characterized by the O−O−O−N dihedral angle (τ_a=25.9°). In fact, such pyramidalization may move toward two reversed directions. This gives two chrial isomers of S_1-min. Two N−O bonds stretch to longer

DOI:10.1063/1674-0068/cjcp2201013

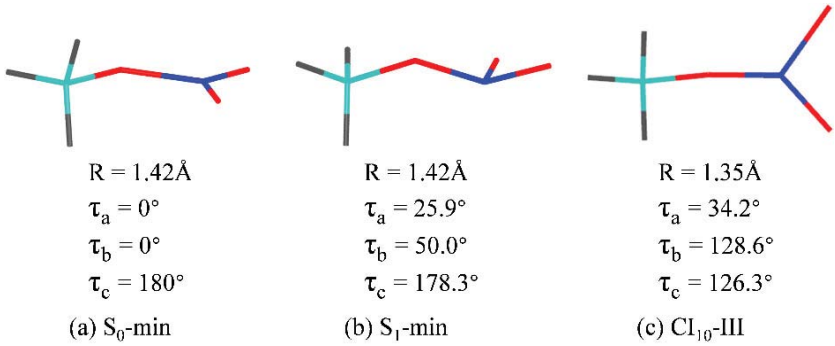

FIG. 2 The geometries of (a) S_0-min and (b) S_1-min of CH_3ONO_2 at the B3LYP/6-311+G(d) level and ADC(2)/def2-TZVP level, respectively. (c) The minimum-energy conicalintersections (MECIs) between S_0 and S_1 (CI_{10}-III) optimized at the SA(4)-CASSCF(12,9)/cc-pVDZ level.

TABLE I The vertical excitation energies, oscillator strengths (f) of S_1, S_2, S_3 and transition orbitals at S_0-min calculated at the ADC(2) level.

Trajectory	Energy/eV	f	Transition orbitals
$S_0 \rightarrow S_1$	4.74	0.0001	
$S_0 \rightarrow S_2$	5.76	0.0003	
$S_0 \rightarrow S_3$	6.42	0.0632	

distances, 1.36 Å and 1.27 Å. The energies of S_0, S_1, S_2 and S_3 at S_1-min with respect to the S_0 energy of S_0-min are 2.19, 3.16, 5.36, and 5.53 eV, respectively.

B. Nonadiabatic dynamics

By using on-the-fly TSH dynamics, we simulated the nonadiabatic dynamics of CH_3ONO_2 starting from different excited states, including S_1, S_2, and S_3, and their time-dependent populations are shown in FIG. 3. When the trajectories start from S_1 (FIG. 3(a)), the S_1 population decay starts at 20 fs and it decreases to 50% at 30 fs. At 40−50 fs, most trajectories jump back to S_0 and the nonadiabatic decay is essentially over. In the whole dynamics process, both S_2 and S_3 do not play important roles here.

When the trajectories start from the S_2 state (FIG. 3(b)), the S_3 state is quickly populated at the very beginning of the dynamics. Afterwards, both S_2 and S_3 populations decay obviously, and the S_1 population rises. At ∼20 fs, the S_0 state population starts to emerge. At ∼45 fs, almost 50% trajectories go back to the S_0 state. At 70 fs, nonadiabatic decay nearly finishes.

When the dynamics starts from S_3 state (FIG. 3(c)), the initial S_3 population decay is observed at the early time of dynamics. At ∼12 fs, the S_0 population starts to rise. At ∼40 fs, it increases to 50%, and at ∼70 fs most trajectories decay to the ground state.

Next, we analyzed the geometrical features at the first S_1/S_0 hopping events in the dynamics, as shown in FIG. 4(a−c). In almost all situations, the strong pyramidalization at the N atom and the elongation of the CH_3O-NO_2 bond were observed. When trajectories initialize from S_1, most hopping geometries are characterized by the longer CH_3O-NO_2 distance and the strong pyramidalization at the N atom (τ_a=22.3°−48.6°). In addition, it is noticed that there is almost a linear relationship between R and τ_a. The linear relationship of R and τ_a for all hopping geometries means that the conical intersection is not a point but a seam in the high dimensional space, and this feature is common in the excited-state nonadiabatic dynamics.

When the trajectories start from S_2, the distribution of R and τ_a becomes more delocalized at the S_1/S_0 hops, although their linear relationship still seems to exist, as shown in FIG. 4(b). The R values are between 1.27 and 3.10 Å, and more hops happen at the long R distance (>2 Å). When the trajectories are put into S_3, the hopping geometry distribution for the values of R and τ_a becomes more delocalized.

To understand the photolysis mechanism at the ADC(2) level, we calculated the PESs between S_0-min and S_1-min using the linear-interpolated method, as

DOI:10.1063/1674-0068/cjcp2201013

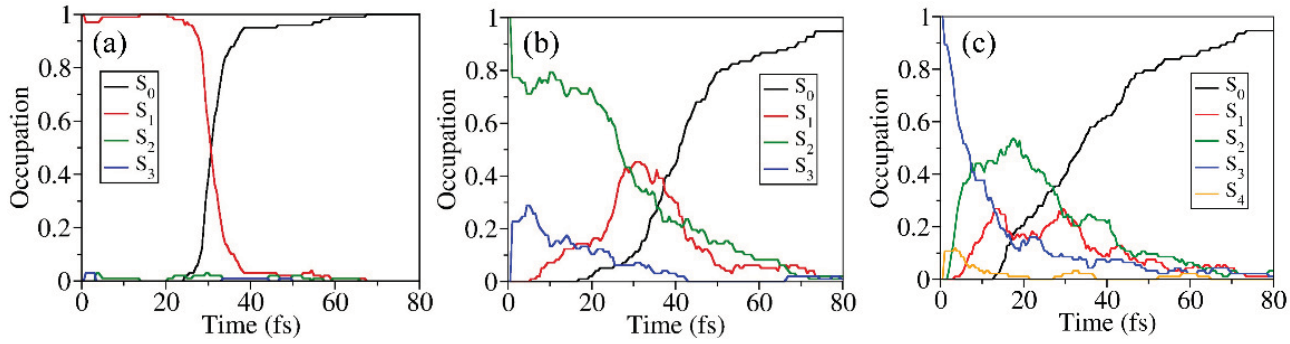

FIG. 3 Time-dependent average fractional occupations in the nonadiabatic dynamics calculated at ADC(2)/def2-TZVP level starting from (a) S_1, (b) S_2, and (c) S_3.

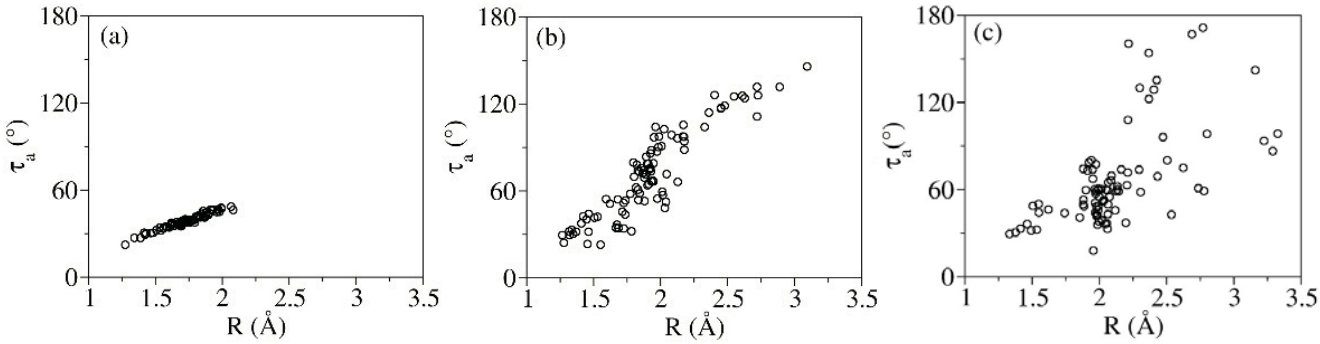

FIG. 4 Two-dimensional geometric distribution at the first $S_1 \rightarrow S_0$ hops at the ADC(2)/def2-TZVP level initialized from (a) S_1, (b) S_2, and (c) S_3.

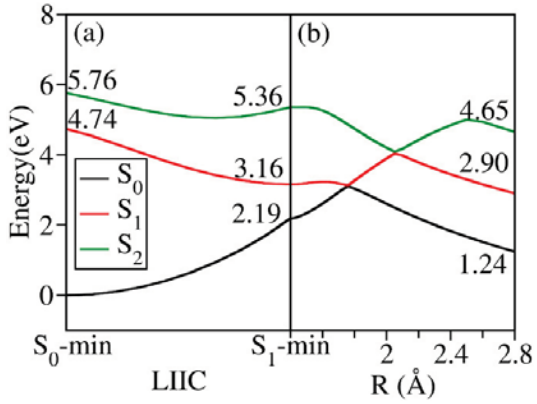

FIG. 5 PESs at the ADC(2)/def2-TZVP levels: (a) linear-interpolated PESs between S_0-min and S_1-min, (b) along with the stretching of the CH_3O-NO_2 bond at the optimized S_1 geometry.

shown in FIG. 5(a). From S_0-min to S_1-min, the system displays strong pyramidalization at the N atom. Starting from S_1-min, we performed the rigid scan of the PESs along with the stretching motion of the CH_3O-NO_2 bond, and an S_1/S_0 crossing exists at R=1.8 Å. Overall, it is clear that the system may easily access the S_1/S_0 PES crossing from the Franck-Condon region. This explains the important roles of the strong pyramidalization and the CH_3O-NO_2 bond stretching motion in the excited-state dynamics of CH_3ONO_2.

Since the excited-state energies are very high, the excessive energy of the system always drives the system into the dissociation channels. Through analyzing the hopping structure distribution, we realize that most trajectories decay to the ground state first and then the dissociation happens. At the ADC(2) level, we always get the CH_3O+NO_2 dissociation channel without the current simulation time duration, no matter which excited state is initialized.

C. Discussions on the ADC(2) results

As the nonadiabatic dynamics of CH_3ONO_2 was simulated at the XMS-CASPT2 level in our previous work [37], we tried to compare the results obtained at the ADC(2) and XMS-CASPT2 levels.

The single-point excited state calculations of ground-state minimum-energy geometry at the XMS-CASPT2 level are comparable to that obtained at the ADC(2)

DOI:10.1063/1674-0068/cjcp2201013

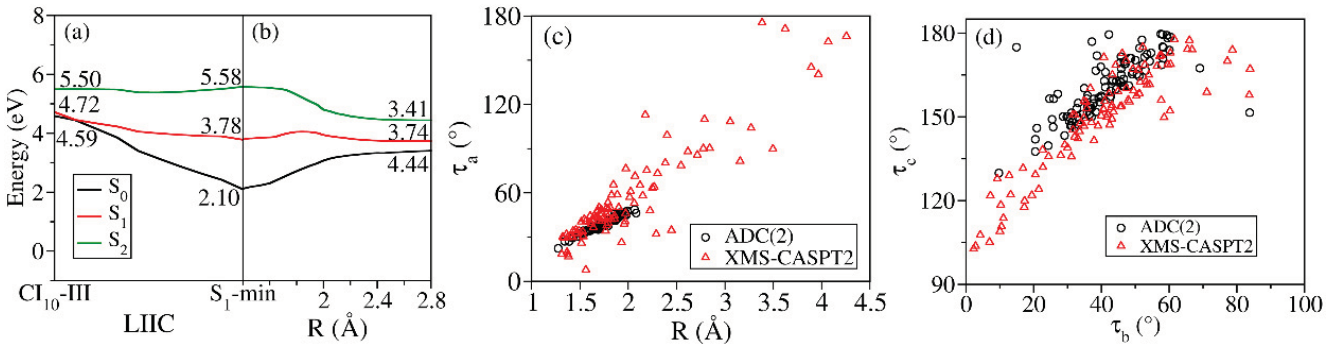

FIG. 6 PESs at the XMS-CASPT2(12,9)/def2-SVPD level: (a) linear-interpolated PESs between CI_{10}-III and S_1-min, (b) along with the stretching of the CH_3O-NO_2 bond at the optimized S_1 geometry. Two-dimensional geometric distribution at the first S_1 to S_0 hops at the ADC(2)/def2-TZVP and XMS-CASPT2(12,9)/def2-SVPD levels [37]: (c) R and τ_a, (d) τ_b and τ_c.

level, such as transition characters and excitation energies. The optimized geometries of S_1-min optimized at these two levels are also very similar.

In the simulation of excited-state nonadiabatic dynamics at both ADC(2) and XMS-CASPT2 levels, the simulation time stops at 250 fs. In both calculations, the population decay manifests that the lifetime of the excited state is very short and the nonadiabatic dynamics finishes before 250 fs. Both two levels give very similar overall population dynamics, no matter whether S_1, S_2, or S_3 are initially excited, indicating that the excited-state pathways should be almost barrierless from the Franck-Condon region to the S_1/S_0 PES crossing.

At the ADC(2) level, before S_1/S_0 hops, the system does not dissociate on the excited state. As shown in FIG. 4(a), the elongation of the CH_3O-NO_2 bond is observed in most hopping geometries, while the bond is still not fully broken. Thus, the decay to the ground state via conical intersections takes place before the dissociation. After internal conversion, the system moves on the ground-state PES. In principle, the system may go back to the equilibrium geometry of the ground state or move to the dissociation limit. However, when the hops at conical intersections take place, the CH_3O-NO_2 bond elongation is observed. Thus, the excessive energy should continue to push the CH_3O-NO_2 bond stretching motion, resulting in the opening of the CH_3O-NO_2 bond dissociation channel. At the same time, the current system is quite small and the initial energy is very high. In this case, only a few degrees of freedom are involved in the vibrational relaxation and thus the dissipation effect should be rather minor. As the consequence, most trajectories directly moves towards the CH_3O-NO_2 dissociation channel.

At the XMS-CASPT2 level, we obtain the PESs between S_1-min and the most important S_1/S_0 CI, and the PESs along with the O−N distance, as shown in FIG. 6 (a) and (b). We also give the key geometrical features at hops, see FIG. 6 (c) and (d).

Some deviations exist when we compared the distribution patterns of the first S_1/S_0 hopping geometries obtained at ADC(2) and XMS-CASPT2 levels. Such differences are also highly relevant to which electronic state the dynamics starts from. Taking the dynamics from the S_1 state as an example, at both levels, the dominant molecular motions are CH_3O-NO_2 bond stretching and strong pyramidalization at the N atom, when the system moves on the excited-state PES from the Franck-Condon region to the S_1/S_0 PES crossing. However, the hopping geometry distribution for the values of R and τ_a becomes more delocalized at the XMS-CASPT2 level. For instance, more hops may take place at the geometries with the long CH_3O-NO_2 bond (R>3 Å) at the XMS-CASPT2 level [37]. Such deviation becomes more pronounced when the dynamics starts from higher excited states. This indicates that both methods may predict the similar excited-state reaction pathways and dominant nuclear degrees of freedom in the nonadiabatic decay, although some detailed topologies of the PESs are different. At the same time, different hopping distribution is also due to that the S_1/S_0 CI topology is not properly treated at the ADC(2) level of theory.

Different features in the TSH dynamics at two levels are attributed by their PESs. For instance, starting from S_1-min, the CH_3O-NO_2 bond prolongation may directly give a S_1/S_0 crossing point at the ADC(2) level (FIG. 5), while the same motion does not result

DOI:10.1063/1674-0068/cjcp2201013

in the S_1/S_0 conical intersection at the XMS-CASPT2 level (FIG. 6(b)). Other molecular motions, including the stronger pyramidalization at the N atom and the torsional motion along the CH_3O-NO_2 bond must be involved in the pathways towards the S_1/S_0 conical intersections (FIG. 2). This explains the reasons that the hopping geometries at the XMS-CASPT2 level show the larger pyramidalization motion at the N atom, with respect to the ADC(2) results. At the same time, the torsional motion along the CH_3O-NO_2 bond is also important for the hops at the XMS-CASPT2 level. This indicates that the dynamics details are not exactly the same at the ADC(2) and XMS-CASPT2 levels. However, starting from S_1 and S_2, the similar excited-state lifetime and dissociation products are identified by using two electronic-structure levels. Some major geometrical features, particularly the obvious pyramidalization motion at the N atom, are also captured by the ADC(2) level. Thus we still think that the results at the ADC(2) level are qualitatively reasonable, although some dynamics details may be different.

At the ADC(2) level, we only obtain the CH_3O+NO_2 photoproduct within the current simulation time duration when the dynamics starts from the S_1, S_2, and S_3 state. The different results are found at the XMS-CASPT2 level, in which the system mainly gives CH_3O+NO_2 channel when starting from S_1 and S_2, and CH_3O+NO_2 and $CH_3O+NO+O$ channels become equally important when initialized from S_3 [37]. At the dissociation limit, the system is composed of two radicals, $CH_3O\cdot+NO_2\cdot$. The $CH_3O\cdot$ fragment shows the C_{3v} symmetry [82, 83]. Due to the very weak Jahn-Teller effects, such radical shows the multi-reference character. In addition, when the O−N bond of NO_2 breaks, the dissociation products even show triplet degeneracy due to the presence of the degenerated p orbitals of the O fragment, giving the strong multi-reference character. As a single-reference method, the ADC(2) method may not give the proper description on such high degenerated case. This explains that the ADC(2) level does not give the correct dissociation channel ($CH_3O+NO+O$).

Overall, the ADC(2) method may give the correct description of the dissociation channels at the low-wavelength excitation, while it cannot treat the photolysis dynamics from the high electronic states.

IV. CONCLUSION

In this work, we simulated the excited-state nonadiabatic dynamics of CH_3ONO_2 using the on-the-fly TSH method at the ADC(2)/def2-TZVP level. We mainly discussed the nonadiabatic decay dynamics of CH_3ONO_2 and examined the performance of ADC(2) theory in the CH_3ONO_2 molecule.

No matter which excited state is initialized, both XMS-CASPT2 and ADC(2) predict the ultrafast decay processes. All simulations indicate that the vibrational motion of the CH_3O-NO_2 bond and the strong pyramidalization at the N atom play critical roles in the excited-state dynamics. However, more degrees of freedom are involved in the TSH dynamics at the XMS-CASPT2 level and thus the geometric distribution at hops is rather dispersed.

The photolysis products are consistent with the experimental study simulated at the long-wavelength (>220 nm), it only gives CH_3O+NO_2. However, other channels are not found, not like the XMS-CASPT2 level. Although the ADC(2) method may not capture the dissociation channels at the short-wavelength excitation, it still gives some acceptable results to understand the photolysis mechanism of CH_3ONO_2 in the cases of low-energy UV excitations. Overall, the ADC(2) level may be useful for treating the nonadiabatic dynamics driven by the low-lying excited-state PES of other similar molecular systems, particularly when such systems contain too many atoms to be treated by the multi-reference electronic-structure methods due to the large computational cost.

V. ACKNOWLEDGMENTS

This work was supported by the National Natural Science Foundation of China (No.21933011, No.21873112). The authors thank the Supercomputing Center, Computer Network Information Center, Chinese Academy of Sciences, the National Supercomputing Center in Shenzhen for providing computational resources.

[1] A. R. Ravishankara, Y. Rudich, and J. A. Pyle, Chem. Rev. **115**, 3679 (2015).
[2] A. E. Perring, S. E. Pusede, and R. C. Cohen, Chem. Rev. **113**, 5848 (2013).
[3] T. K. Minton, C. M. Nelson, T. A. Moore, and M. Okumura, Science **258**, 1342 (1992).
[4] A. Prlj, L. M. Ibele, E. Marsili, and B. F. E. Curchod, J. Phys. Chem. Lett. **11**, 5418 (2020).

DOI:10.1063/1674-0068/cjcp2201013

[5] I. Barnes, K. H. Becker, and T. Zhu, J. Atmos. Chem. **17**, 353 (1993).
[6] W. Xiang, X. Y. Zhang, K. Q. Chen, J. E. Fang, F. He, X. Hu, D. C. W. Tsang, Y. S. Ok, and B. Gao, Chem. Eng. J. **385**, 123842 (2020).
[7] K. N. Lin, D. P. Hu, J. W. Peng, C. Xu, F. L. Gu, and Z. G. Lan, Chemosphere **281**, 130831 (2021).
[8] D. Shemesh, S. A. Nizkorodov, and R. B. Gerber, J. Phys. Chem. A **120**, 7112 (2016).
[9] D. Shemesh, Z. G. Lan, and R. B. Gerber, J. Phys. Chem. A **117**, 11711 (2013).
[10] R. Atkinson, W. P. L. Carter, and A. M. Winer, J. Phys. Chem. **87**, 2012 (1983).
[11] E. L. Derro, C. Murray, M. I. Lester, and M. D. Marshall, Phys. Chem. Chem. Phys. **9**, 262 (2007).
[12] W. D. Taylor, T. D. Allston, M. J. Moscato, G. B. Fazekas, R. Kozlowski, and G. A. Takacs, Int. J. Chem. Kinet. **12**, 231 (1980).
[13] R. M. Moore and N. V. Blough, Geophys. Res. Lett. **29**, 1737 (2002).
[14] X. F. Yang, P. Felder, and J. R. Huber, J. Phys. Chem. **97**, 10903 (1993).
[15] A. L. Chuck, S. M. Turner, and P. S. Liss, Science **297**, 1151 (2002).
[16] M. P. Turberg, D. M. Giolando, C. Tilt, T. Soper, S. Mason, M. Davies, P. Klingensmith, and G. A. Takacs, J. Photochem. Photobiol. A **51**, 281 (1990).
[17] D. E. Shallcross, P. Biggs, C. E. Canosa-Mas, K. C. Clemitshaw, M. G. Harrison, M. R. L. Alañón, J. A. Pyle, A. Vipond, and R. P. Wayne, J. Chem. Soc. Faraday Trans. **93**, 2807 (1997).
[18] R. K. Talukdar, J. B. Burkholder, M. Hunter, M. K. Gilles, J. M. Roberts, and A. R. Ravishankara, J. Chem. Soc. Faraday Trans. **93**, 2797 (1997).
[19] R. K. Talukdar, S. C. Herndon, J. B. Burkholder, J. M. Roberts, and A. R. Ravishankara, J. Chem. Soc. Faraday Trans. **93**, 2787 (1997).
[20] A. Bacak, M. W. Bardwell, M. T. Raventos, C. J. Percival, G. Sanchez-Reyna, and D. E. Shallcross, J. Phys. Chem. A **108**, 10681 (2004).
[21] A. Lesar, M. Hodošček, E. Drougas, and A. M. Kosmas, J. Phys. Chem. A **110**, 7898 (2006).
[22] J. Soto, D. Peláez, J. C. Otero, F. J. Avila, and J. F. Arenas, Phys. Chem. Chem. Phys. **11**, 2631 (2009).
[23] P. G. Carbajo and A. J. Orr-Ewing, Phys. Chem. Chem. Phys. **12**, 6084 (2010).
[24] S. Z. He, Z. M. Chen, and X. Zhang, Environ. Chem. **8**, 529 (2011).
[25] A. Dey, R. Fernando, C. Abeysekera, Z. Homayoon, J. M. Bowman, and A. G. Suits, J. Chem. Phys. **140**, 054305 (2014).
[26] C. M. Higgins, L. A. Evans, G. C. Lloyd-Jones, D. E. Shallcross, D. P. Tew, and A. J. Orr-Ewing, J. Phys. Chem. A **118**, 2756 (2014).
[27] J. E. Williams, G. Le Bras, A. Kukui, H. Ziereis, and C. A. M. Brenninkmeijer, Atmos. Chem. Phys. **14**, 2363 (2014).
[28] J. M. Roberts and R. W. Fajer, Environ. Sci. Technol. **23**, 945 (1989).
[29] W. Domcke, D. R. Yarkony, and H. Köppel, *Conical Intersections: Electronic Structure, Dynamics and Spectroscopy*, Singapore: World Scientific Publishing Company (2004).
[30] W. Domcke, D. R. Yarkony, and H. Köppel, *Conical Intersections: Theory, Computation and Experiment*, Singapore: World Scientific Publishing Company (2011).
[31] K. C. Clemitshaw, J. Williams, O. V. Rattigan, D. E. Shallcross, K. S. Law, and R. A. Cox, J. Photochem. Photobiol. A **102**, 117 (1997).
[32] R. E. Rebbert, J. Phys. Chem. **67**, 1923 (1963).
[33] L. Zhu and C. F. Ding, Chem. Phys. Lett. **265**, 177 (1997).
[34] L. Zhu and D. Kellis, Chem. Phys. Lett. **278**, 41 (1997).
[35] W. T. Luke and R. R. Dickerson, Geophys. Res. Lett. **15**, 1181 (1988).
[36] W. T. Luke, R. R. Dickerson, and L. J. Nunnermacker, J. Geophys. Res. **94**, 14905 (1989).
[37] J. J. Zhang, J. W. Peng, D. P. Hu, and Z. G. Lan, Phys. Chem. Chem. Phys. **23**, 25597 (2021).
[38] J. C. Tully, J. Chem. Phys. **93**, 1061 (1990).
[39] J. Finley, P. Å. Malmqvist, B. O. Roos, and L. Serrano-Andrés, Chem. Phys. Lett. **288**, 299 (1998).
[40] K. Andersson, P. Å. Malmqvist, and B. O. Roos, J. Chem. Phys. **96**, 1218 (1992).
[41] T. Shiozaki, W. Győrffy, P. Celani, and H. J. Werner, J. Chem. Phys. **135**, 081106 (2011).
[42] I. Polyak, L. Hutton, R. Crespo-Otero, M. Barbatti, and P. J. Knowles, J. Chem. Theory Comput. **15**, 3929 (2019).
[43] M. Heindl and L. González, Comput. Theor. Chem. **1155**, 38 (2019).
[44] P. J. Knowles and H. J. Werner, Chem. Phys. Lett. **145**, 514 (1988).
[45] H. J. Werner and P. J. Knowles, J. Chem. Phys. **89**, 5803 (1988).
[46] P. J. Knowles and N. C. Handy, Comput. Phys. Commun. **54**, 75 (1989).
[47] H. J. Werner and P. J. Knowles, J. Chem. Phys. **82**, 5053 (1985).
[48] H. Lischka, D. Nachtigallová, A. J. A. Aquino, P. G. Szalay, F. Plasser, F. B. C. Machado, and M. Barbatti, Chem. Rev. **118**, 7293 (2018).
[49] J. W. Park, R. Al-Saadon, M. K. MacLeod, T. Shiozaki, and B. Vlaisavljevich, Chem. Rev. **120**, 5878 (2020).
[50] A. Koslowski, M. E. Beck, and W. Thiel, J. Comput.

DOI:10.1063/1674-0068/cjcp2201013

Chem. **24**, 714 (2003).
[51] M. Barbatti and H. Lischka, J. Am. Chem. Soc. **130**, 6831 (2008).
[52] X. H. Zhuang, J. Wang, and Z. G. Lan, J. Phys. Chem. B **117**, 15976 (2013).
[53] Z. G. Lan, E. Fabiano, and W. Thiel, J. Phys. Chem. B **113**, 3548 (2009).
[54] N. Otte, M. Scholten, and W. Thiel, J. Phys. Chem. A **111**, 5751 (2007).
[55] E. Runge and E. K. U. Gross, Phys. Rev. Lett. **52**, 997 (1984).
[56] E. K. U. Gross and W. Kohn, Phys. Rev. Lett. **55**, 2850 (1985).
[57] A. B. Trofimov and J. Schirmer, J. Phys. B: At. Mol. Opt. Phys. **28**, 2299 (1995).
[58] J. Schirmer, Phys. Rev. A **26**, 2395 (1982).
[59] E. Tapavicza, I. Tavernelli, U. Rothlisberger, C. Filippi, and M. E. Casida, J. Chem. Phys. **129**, 124108 (2008).
[60] K. Tomić, J. Tatchen, and C. M. Marian, J. Phys. Chem. A **109**, 8410 (2005).
[61] B. G. Levine, C. Ko, J. Quenneville, and T. J. Martnez, Mol. Phys. **104**, 1039 (2006).
[62] D. P. Hu, Y. F. Liu, A. L. Sobolewski, and Z. G. Lan, Phys. Chem. Chem. Phys. **19**, 19168 (2017).
[63] D. Tuna, D. Lefrancois, Ł. Wolański, S. Gozem, I. Schapiro, T. Andruniów, A. Dreuw, and M. Olivucci, J. Chem. Theory Comput. **11**, 5758 (2015).
[64] H. H. Teh and J. E. Subotnik, J. Phys. Chem. Lett. **10**, 3426 (2019).
[65] S. Matsika, Chem. Rev. **121**, 9407 (2021).
[66] L. Stojanović, S. M. Bai, J. Nagesh, A. F. Izmaylov, R. Crespo-Otero, H. Lischka, and M. Barbatti, Molecules **21**, 1603 (2016).
[67] F. Plasser, R. Crespo-Otero, M. Pederzoli, J. Pittner, H. Lischka, and M. Barbatti, J. Chem. Theory Comput. **10**, 1395 (2014).
[68] L. González, D. Escudero, and L. Serranoés, Chemphyschem **13**, 28 (2012).
[69] L. Martínez-Fernández, L. González, and I. Corral, Comput. Theor. Chem. **975**, 13 (2011).
[70] J. Huang, L. K. Du, J. Wang, and Z. G. Lan, J. Phys. Chem. C **119**, 7578 (2015).
[71] L. K. Du and Z. G. Lan, J. Chem. Theory Comput. **11**, 1360 (2015).
[72] A. Prlj, B. F. E. Curchod, and C. Corminboeuf, Phys. Chem. Chem. Phys. **17**, 14719 (2015).
[73] B. Milovanović, J. Novak, M. Etinski, W. Domcke, and N. Došlić, Phys. Chem. Chem. Phys. **23**, 2594 (2021).
[74] E. Marsili, A. Prlj, and B. F. E. Curchod, Phys. Chem. Chem. Phys. **23**, 12945 (2021).
[75] M. J. Frisch, G. W. Trucks, H. B. Schlegel, G. E. Scuseria, M. A. Robb, J. R. Cheeseman, G. Scalmani, V. Barone, G. A. Petersson, H. Nakatsuji, X. Li, M. Caricato, A. V. Marenich, J. Bloino, B. G. Janesko, R. Gomperts, B. Mennucci, H. P. Hratchian, J. V. Ortiz, A. F. Izmaylov, J. L. Sonnenberg, D. Williams-Young, F. Ding, F. Lipparini, F. Egidi, J. Goings, B. Peng, A. Petrone, T. Henderson, D. Ranasinghe, V. G. Zakrzewski, J. Gao, N. Rega, G. Zheng, W. Liang, M. Hada, M. Ehara, K. Toyota, R. Fukuda, J. Hasegawa, M. Ishida, T. Nakajima, Y. Honda, O. Kitao, H. Nakai, T. Vreven, K. Throssell, J. A. Montgomery Jr., J. E. Peralta, F. Ogliaro, M. J. Bearpark, J. J. Heyd, E. N. Brothers, K. N. Kudin, V. N. Staroverov, T. A. Keith, R. Kobayashi, J. Normand, K. Raghavachari, A. P. Rendell, J. C. Burant, S. S. Iyengar, J. Tomasi, M. Cossi, J. M. Millam, M. Klene, C. Adamo, R. Cammi, J. W. Ochterski, R. L. Martin, K. Morokuma, O. Farkas, J. B. Foresman, and D. J. Fox, *Gaussian 16, Revision C.01*, Wallingford, CT: Gaussian Inc. (2016).
[76] E. Wigner, Phys. Rev. **40**, 749 (1932).
[77] C. Y. Zhu, S. Nangia, A. W. Jasper, and D. G. Truhlar, J. Chem. Phys. **121**, 7658 (2004).
[78] G. Granucci and M. Persico, J. Chem. Phys. **126**, 134114 (2007).
[79] L. K. Du and Z. G. Lan, J. Chem. Theory Comput. **11**, 4522 (2015).
[80] R. Ahlrichs, M. Bär, M. Häser, H. Horn, and C. Kölmel, Chem. Phys. Lett. **162**, 165 (1989).
[81] A. M. Launder, J. Agarwal, and H. F. Schaefer III, J. Chem. Phys. **143**, 234302 (2015).
[82] C. F. Jackels, J. Chem. Phys. **76**, 505 (1982).
[83] T. A. Barckholtz and T. A. Miller, J. Phys. Chem. A **103**, 2321 (1999).

DOI:10.1063/1674-0068/cjcp2201013